the plant journal

SEB Society for Experimental Biology

The Plant Journal (2017) **89,** 112–127 doi: 10.1111/tpj.13326

PP2A-B′γ modulates foliar *trans*-methylation capacity and the formation of 4-methoxy-indol-3-yl-methyl glucosinolate in Arabidopsis leaves

Moona Rahikainen[1,†], Andrea Trotta[1,†], Sara Alegre[1], Jesús Pascual[2], Katariina Vuorinen[3], Kirk Overmyer[3], Barbara Moffatt[4], Stéphane Ravanel[5], Erich Glawischnig[6] and Saijaliisa Kangasjärvi[1,*]

[1]*Department of Biochemistry, Molecular Plant Biology, University of Turku, FI-20014 Turku, Finland,*

[2]*Plant Physiology Lab, Organisms and Systems Biology, Faculty of Biology, University of Oviedo, Oviedo, Asturias, Spain,*

[3]*Division of Plant Biology, Department of Biosciences, Viikki Plant Science Centre, University of Helsinki, Helsinki, Finland,*

[4]*Department of Biology, University of Waterloo, 200 University Avenue, Ontario N2L 3G1, Canada,*

[5]*Laboratoire de Physiologie Cellulaire et Végétale, CNRS UMR5168, INRA UMR1417, CEA, Université Grenoble Alpes, 38054 Grenoble, France, and*

[6]*Department of Plant Sciences, Technische Universität München, Emil-Ramann-Str.4 85354, Freising, Germany*

Received 12 February 2016; revised 31 August 2016; accepted 1 September 2016; published online 5 December 2016.

*For correspondence (e-mail Saijaliisa.kangasjarvi@utu.fi).

†These authors contributed equally to this work.

SUMMARY

Glucosinolates (GSL) of cruciferous plants comprise a major group of structurally diverse secondary compounds which act as deterrents against aphids and microbial pathogens and have large commercial and ecological impacts. While the transcriptional regulation governing the biosynthesis and modification of GSL is now relatively well understood, post-translational regulatory components that specifically determine the structural variation of indole glucosinolates have not been reported. We show that the cytoplasmic protein phosphatase 2A regulatory subunit B′γ (PP2A-B′γ) physically interacts with indole glucosinolate methyltransferases and controls the methoxylation of indole glucosinolates and the formation of 4-methoxy-indol-3-yl-methyl glucosinolate in Arabidopsis leaves. By taking advantage of proteomic approaches and metabolic analysis we further demonstrate that PP2A-B′γ is required to control the abundance of oligomeric protein complexes functionally linked with the activated methyl cycle and the *trans*-methylation capacity of leaf cells. These findings highlight the key regulatory role of PP2A-B′γ in methionine metabolism and provide a previously unrecognized perspective for metabolic engineering of glucosinolate metabolism in cruciferous plants.

Keywords: protein phosphatase 2A, glucosinolate, activated methyl cycle, *Arabidopsis thaliana*.

INTRODUCTION

Stress-induced reprogramming of primary metabolism and the production of secondary metabolites are essential defense mechanisms that prevent pathogens and pests from colonizing host plant tissues (Smith and Clement, 2012). These metabolic rearrangements are tightly connected with biosynthesis and recycling of amino acids, which provide precursors for a variety of secondary compounds, and hence connect light-driven biosynthetic processes with biotic stress resistance in plants (Trotta *et al.*, 2014). Methionine metabolism is tightly connected with primary and secondary sulfur metabolism in plants, and methionine is one of the essential amino acids in human nutrition. The level of free methionine depends on sulfur assimilation and *de novo* methionine biosynthesis in chloroplasts, as well as on the recycling of methionine in the 'activated methyl cycle' in the cytoplasm (Ravanel *et al.*, 2004). Methionine acts as a precursor for the universal methyl donor *S*-adenosyl-L-methionine (SAM), which is essential in numerous *trans*-methylation reactions ranging from basic metabolism and gene regulation to biosynthesis of a wide range of natural compounds with complex chemical structures (Ravanel *et al.*, 1998; Amir, 2010). The centrality of *trans*-methylation reactions is reflected by *in vivo* flux measurements indicating that the synthesis

and turnover of SAM can account for up to 80% of methionine metabolism in plant cells (Giovanelli *et al.*, 1985)

In cruciferous plants of the Brassicaceae family like *Arabidopsis thaliana* (hereafter Arabidopsis), methionine metabolism is tightly linked with the biosynthesis of aliphatic methionine-derived and indole tryptophan-derived glucosinolates (GSLs), major secondary compounds that confer resistance against insect herbivores and microbial pathogens (Sønderby *et al.*, 2010). In response to biotic stress, indole GSLs undergo hydroxylation and *trans*-methylation reactions and the resulting modified GSLs display diverse biological functions. For example, post-ingestion breakdown of indole GSL inhibits feeding by green peach aphid (*Myzus persicae*) (Kim and Jander, 2007). In response to *Pseudomonas syringae* infection, degradation of methoxylated indole GSL by the myrosinase penetration 2 (PEN2) (Bednarek *et al.*, 2009) in turn triggers callose deposition into the cell wall (Clay *et al.*, 2009). Recently, Xu *et al.* (2016) showed that infection by the necrotrophic fungal pathogen *Botrytis cinerea* promotes the biosynthesis of indole GSLs and their conversion to methoxylated intermediates, which are further metabolized to unstable antimicrobial compounds by PEN2. The beta-thioglucoside glucosidases TGG1 and TGG2 have also recently been implicated in the degradation of indole GSLs and shown to attenuate cell death caused by the detrimental fungal toxin fumonisin B1 (Zhao *et al.*, 2015). GSLs are also of major economic importance, because specifically decorated GSLs affect the taste of cruciferous crops and have both health-promoting and deleterious effects in the human diet (Halkier and Gershenzon, 2006; Agerbirk *et al.*, 2009). Biotechnological manipulation of methionine metabolism, however, is still limited by incomplete understanding of the underlying metabolic networks.

Stress-induced biosynthetic processes, such as the methoxylation of hydroxylated indole GSLs, form a significant sink for SAM and necessitate tight regulation of the activated methyl cycle (Bekaert *et al.*, 2012). The recycling of the toxic and inhibitory reaction product *S*-adenosylhomocysteine (SAH) and re-synthesis of SAM are critical in maintaining the activity of SAM-dependent methyltransferases. To prevent its toxic effect, SAH is continuously hydrolyzed by *S*-adenosylhomocysteine hydrolase (SAHH), making this an essential step in methionine metabolism (Moffatt and Weretilnyk, 2001). The reaction product, homocysteine (HCy), is converted back to methionine by cytosolic cobalamine-independent methionine synthase (CIMS) in a methyl-tetrahydrofolate (Me-THF)-dependent reaction. Me-THF derives from the reduction of methylene-THF through a reaction catalyzed by methylene-THF reductase (MTHFR) in the cytosol (Roje *et al.*, 1999) and is the most abundant folate derivative in light-exposed leaves (Van Wilder *et al.*, 2009).

In previous studies we found that a specific cytoplasmic protein phosphatase 2A regulatory subunit B′γ (PP2A-B′γ) is required to control light-dependent oxidative stress-induced metabolite signatures in Arabidopsis leaves (Trotta *et al.*, 2011; Li *et al.*, 2014). Proteomic approaches revealed that *pp2a-b′γ* mutants accumulate phosphorylated SAHH and the myrosinase TGG1 in distinct oligomeric complexes, presumably to facilitate defense-associated metabolism (Trotta *et al.*, 2011; Li *et al.*, 2014). Such adjustments could be key to the increased resistance of *pp2a-b′γ* against *B. cinerea* (Trotta *et al.*, 2011) and reduced fecundity of green peach aphid on *pp2a-b′γ* as compared with wild-type plants (Rasool *et al.*, 2014). In this research we set out to specify PP2A-B′γ-dependent adjustments in methionine metabolism. By analyzing protein interactions, 1D and 3D gel-based proteomic approaches and targeted metabolic analysis, we demonstrate that PP2A-B′γ exerts a control over the abundance of SAHH and CIMS in oligomeric protein complexes and modulates the *trans*-methylation capacity of leaf cells. Associated with these protein interactions and metabolic adjustments, PP2A-B′γ is shown to interact with indole glucosinolate methyl transferase isoforms 1 and 4 (IGMT1 and IGMT4) and control the methoxylation of indole GSLs in Arabidopsis leaves.

RESULTS

PP2A-B′γ interacts with IGMTs

To gain insight into the functional role of PP2A-B′γ in the regulation of methionine metabolism, we took advantage of yeast two-hybrid screening using PP2A-B′γ as bait against a cDNA library constructed using differentially stress-exposed tissues (Jaspers *et al.*, 2009; Konert *et al.*, 2015a). The PCR analysis revealed that two of the 35 positive colonies expressed IGMT4 (AT1G21130) as a candidate interactor for PP2A-B′γ. IGMT4 belongs to a family of four closely related enzymes with 95% amino acid identity (Figure 1a) (Pfalz *et al.*, 2011). The positive yeast colonies contained sequences that correspond to the N-terminal domain of IGMT4, which harbors a putative dimerization domain and differs from IGMT1, -2 and -3 by 11, 10 and 12 amino acids within the first 133 N-terminal amino acids, respectively (Figure 1a).

To assess the presence of IGMTs in non-stress-exposed Arabidopsis leaves, we isolated total foliar soluble extracts from the wild type, *pp2a-b′γ* and a *pp2a-b′γ* line complemented by 35S-driven expression of the *PP2A-B′γ* gene. The proteins were separated on 12% polyacrylamide gel, and a band containing polypeptides migrating at approximately 40 kDa, corresponding to the molecular weights of IGMT1–IGMT4, was cut out from a Coomassie-stained gel and subjected to in-gel trypsin digestion. Subsequent data-dependent nanoscale liquid chromatography/electrospray ionization tandem mass spectrometry (nLC/ESI-MS/MS)

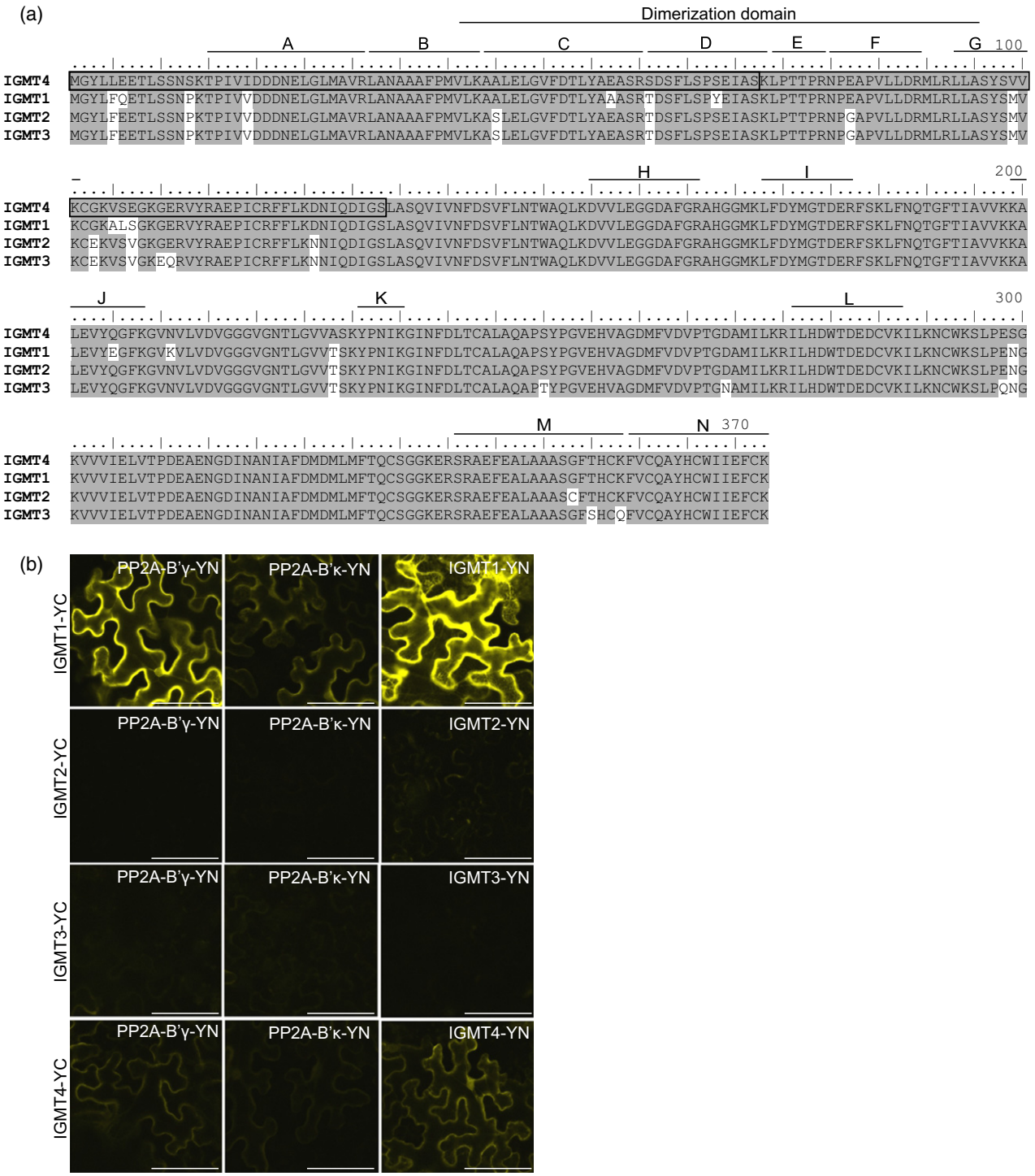

Figure 1. Interaction between protein phosphatase 2A regulatory subunit B′γ (PP2A-B′γ) and indole glucosinolate methyltransferase (IGMT).
(a) Amino acid sequence alignment of the Arabidopsis IGMT family. The N-terminal IGMT4 peptides (amino acids 1–72 and 1–133) identified in a yeast two-hybrid screen using PP2A-B′γ as the bait are indicated with back frames. Amino acids identical for IGMT1–IGMT4 are shaded in grey. The dimerization domain (Pfam) is indicated. The letters A–N indicate peptides detected in MS analysis as specified in Table 1.
(b) Bimolecular fluorescence complementation analysis of protein interactions in *Nicotiana benthamiana* leaves transiently expressing IGMT1-YC, IGMT2-YC, IGMT3-YC, IGMT4-YC and PP2A-B′γ-YN, PP2A-B′κ-YN or IGMT1-YN, IGMT2-YN, IGMT3-YN and IGMT4-YN fusion proteins under the 35S promoter. Scale bars correspond to 100 μm.

identified a total of 736 proteins from all genotypes, IGMT4 being the 195th hit (Table S1 in the Supporting Information). Four unique peptides were detected for IGMT4 (Figure 1a, Table 1). Additionally, we detected two peptides common to IGMT1 and IGMT4, one peptide common to IGMT1, -2 and -4, one peptide common to IGMT2, -3 and -4, and six peptides common to all four IGMT isoforms. However, peptides unique to IGMT1–IGMT3 were not detected (Table 1). Finally, two additional bands were cut, one right above and one below the 40-kDa band. Subsequent MS analysis did not detect unique IGMT1–IGMT3 peptides in these fractions either (Tables S2 and S3).

The number of peptide spectrum matches (PSMs), which can be used as an indication of protein abundance in a sample, inferred an increased abundance of IGMT4 in *pp2a-b′γ* compared with the wild type or the *pp2a-b′γ* complementation line (Table 1). As a comparison, within the 40-kDa bands, the pathogen-inducible β-1,3-glucanase pathogenesis-related 2 (PR2) was barely detected in the wild type and showed significantly increased abundance in *pp2a-b′γ* (Table 1). Other proteins, such as the highly abundant translational elongation factor, eIF2alpha homolog (AT2G40290), did not show significant changes between the genotypes (Table 1). Taken together, this mass spectrometry approach confirmed the presence of IGMT4 in non-stress-exposed wild-type plants and suggested an increased abundance of IGMT4 in *pp2a-b′γ*. Since unique peptides for IGMT1–IGMT3 were not detected, their presence could not be unequivocally demonstrated.

Next we used bimolecular fluorescence complementation (BiFC), which involves heterologous expression of fusion proteins of interest and allows visualization of interactions that are highly transient in nature. A clear YFP-fluorescence indicative of protein–protein interaction was detected in the epidermal cells of *Nicotiana benthamiana* leaves heterologously expressing the fusion proteins for PP2A-B′γ and IGMT1, and a weaker fluorescent signal in the cells expressing PP2A-B′γ and IGMT4 (Figure 1b). Only faint fluorescence was detected for PP2A-B′γ and IGMT2 or IGMT3 (Figure 1b). The lack of clear PP2A-B′γ–IGMT2/IGMT3 interaction in our experimental system, however, does not fully rule out the possibility that these interactions may still occur under specific physiological conditions. Likewise, only weak fluorescence signals were detected when another regulatory PP2A-B′ subunit, PP2A-B′κ, and IGMT1 or IGMT4 were co-expressed in the transient assay (Figure 1b). Immunoblot analysis confirmed that all the PP2A and IGMT isoforms tested were expressed in the *N. benthamiana* leaves (Figure S1). IGMT1 and IGMT4 also interacted with themselves, which is consistent with the generally observed dimeric nature of *O*-methyltransferases (Figure 1b) (Zubieta *et al.*, 2001).

PP2A-B′γ is required to control the amount of a specifically methoxylated indole glucosinolate 4MO-I3M

The physical interaction between PP2A-B′γ and IGMTs, together with the presence of at least IGMT4 in non-stress-exposed wild-type and *pp2a-b′γ* leaves (Table 1), prompted

Table 1 Indole glucosinolate methyltransferase (IGMT) peptides identified in MS analysis of wild type (WT), *pp2a-b′γ* and *pp2a-b′γ 35S::PP2A-B′γ* samples. Total soluble protein extracts were separated on SDS-PAGE and a band at 40 kDa corresponding to the size of IGMT4 was cut out for analysis by nanoscale liquid chromatography/electrospray ionization tandem mass spectrometry. Letters A–N correspond to the peptides indicated in Figure 1(a). Peptide spectrum matches (PSMs) of IGMT4, pathogenesis-related protein 2 (PR2; AT3G57260) and eukaryotic initiation factor 2α (eIF2α; AT2G40290) are indicated as a sum from two biological replicates

Peptide		Presence in different IGMT isoforms				PSMs		
		IGMT1	IGMT2	IGMT3	IGMT4	WT	*pp2a-b′γ*	*pp2a-b′γ P35S::PP2A-B′γ*
A	TPIVIDDDNELGLMAVR				X	2	5	2
B	LANAAAFPMVLK	X	X	X	X	2	4	4
C	AALELGVFDTLYAEASR				X	0	1	0
D	SDSFLSPSEIASK				X	4	6	4
E	LPTTPR	X	X	X	X	1	0	0
F	NPEAPVLLDR	X			X	6	7	7
G	LLASYSVVK				X	3	5	4
H	DVVLEGGDAFGR	X	X	X	X	1	1	0
I	LFDYMGTDER	X	X	X	X	2	4	3
J	KALEVYQGFK		X	X	X	1	3	1
K	YPNIK	X	X	X	X	7	10	10
L	ILHDWTDEDcVK	X	X	X	X	5	7	6
M	SRAEFEALAAASGFTHcK	X			X	2	4	2
N	FVcQAYHcWIIEFcK	X	X		X	2	4	2
	Total PSMs for IGMT4 (AT1G21130)					38	61	45
	Total PSMs for PR2 (AT3G57260)					2	93	32
	Total PSMs for eIF2a (AT2G40290)					196	226	212

us to analyse the profiles of aliphatic and indole GSLs in the wild type, *pp2a-b′γ* and the *pp2a-b′γ* complementation line. The three most commonly observed indole GSLs of Arabidopsis include indolyl-3-methyl glucosinolate (I3M), 1-methoxy-indol-3-yl-methyl glucosinolate (1MO-I3M) and 4-methoxy-indol-3-yl-methyl glucosinolate (4MO-I3M) (Agerbirk *et al.*, 2009; Pfalz *et al.*, 2011). In three independent experiments, accumulation of 4MO-I3M was consistently observed in 33-day-old *pp2a-b′γ* compared with the wild type or the complementation line (Figure 2b). A slight statistically insignificant corresponding decrease in the amount of I3M was observed in *pp2a-b′γ*; I3M serves as precursor in the two-step reactions leading to the formation of 4MO-I3M and 1MO-I3M, where IGMTs catalyze the second step (Figure 2). The levels of aliphatic GSLs were not consistent and varied between the genotypes in the different experiments (Figure 2e). Hence, we focused on the impact of PP2A-B′γ on the abundance of 4MO-I3M in Arabidopsis leaves.

The *pp2a-b′γ* mutant exhibits constitutive age-dependent defense reactions that become apparent after approximately 4 weeks of age when grown at 50% relative humidity (RH) (Trotta *et al.*, 2011) – at 3 weeks of age no symptoms of premature yellowing in *pp2a-b′γ* leaves could be observed (Figure S2). In high-humidity conditions, the conditional yellowing phenotype of *pp2a-b′γ* is alleviated (Konert *et al.*, 2015b). To understand whether PP2A-B′γ is required to control the GSL content in healthy and/or stressed leaves, we measured the levels of GSLs in non-stress-exposed 19-day-old plants grown at 50% RH as well as in 4-week-old plants grown at 65/75% RH and subsequently infected with *B. cinerea* at 100% RH to facilitate the fungal infection.

Similarly to 33-day-old *pp2a-b′γ*, accumulation of 4MO-I3M was also evident in 19-day-old *pp2a-b′γ* when compared with the wild-type or the complementation line (Figure 2a). Under the high-humidity conditions used in the *B. cinerea* infection assays, however, the mock-treated *pp2a-b′γ* plants did not display an increased 4MO-I3M content when compared with the wild type or the complementation line (Figure 2c). *Botrytis cinerea* infection induced an increase in the amount of 4MO-I3M in all genotypes, and this response was significantly pronounced in *pp2a-b′γ* compared with the wild type or the complementation line (Figure 2c). In all the experimental conditions applied, the ratio between 4MO-I3M and total indole GSL was always significantly higher in *pp2a-b′γ* compared with the wild type or the complementation line (Figure 2d).

PP2A-B′γ modulates the cellular *trans*-methylation potential

The regulatory network controlling the biosynthesis of modified GSLs is tightly linked with primary amino acid metabolism, but the metabolic interactions underlying this network remain poorly understood. Previously, we found increased abundance and differential phosphorylation of enzymes functionally related to the activated methyl cycle and GSL catabolism, such as SAHH1, TGG1 and thiocyanate methyltransferase 1 (also known as harmless to ozone layer 1, HOL1) in *pp2a-b′γ* mutant backgrounds (Trotta *et al.*, 2011; Li *et al.*, 2014). This prompted us to ask whether PP2A-B′γ is required to coordinate the recycling of methionine and SAM in the activated methyl cycle. Hence we next focused on metabolic intermediates of the activated methyl cycle (HCy, methionine, SAM and SAH) in the wild type, *pp2a-b′γ* and the *pp2a-b′γ* complementation line.

Metabolite analysis revealed an increase in the SAM content of *pp2a-b′γ* leaves, whereas the abundance of HCy and SAH did not differ between the genotypes (Figure 3a and b). Since the *pp2a-b′γ* mutation had no significant impact on the level of cysteine and its precursor *O*-acetylserine (Figure 3b), the changes in SAM suggest a perturbation in the activated methyl cycle rather than in the sulfur assimilation pathway. This assumption is supported by previous metabolic analyses showing that the level of glutathione was not modified in the *pp2a-b′γ* mutant compared with the wild type (Li *et al.*, 2014). The increase in SAM in *pp2a-b′γ* leaves was coupled with an increased

Figure 2. Glucosinolate (GSL) profiles of wild-type (WT), *pp2a-b′γ* and *pp2a-b′γ 35S::PP2A-B′γ* complementation lines.
(a)–(c) GSL profiles of WT, *pp2a-b′γ* and *pp2a-b′γ 35S::PP2A-B′γ* complementation lines at the age of 33 days (a) and 19 days (b), and after mock-treatment or infection of 28-day-old plants with *Botrytis cinerea* (c). In (a), the results are means ± SD ($n = 4$) from a representative experiment among three independent measurements. In (b) and (c), the results are means ± SD and $n = 4$. The aliphatic GSLs 3MSOP (3-methylsulfinylpropyl GSL; glucoiberin), 4MSOB (4-methylsulfinylbutyl GSL; glucoraphanin), 4MTB (4-methylthiolbutyl GSL; glucoerucin), 5MSOP (5-methylsulfinylpentyl GSL; glucoalyssin), 8MSOO (8-methylsulfinyloctyl GSL; glucohirsutin) and indole glucosinolates I3M (indol-3-ylmethyl GSL; glucobrassicin), 4MO-I3M (4-methoxyindol-3-ylmethyl GSL; 4-methoxyglucobrassicin) and 1MO-I3M (1-methoxyindol-3-ylmethyl GSL; neoglucobrassicin) are shown. One-way ANOVA followed by Tukey's pairwise comparisons was used to analyse the GSL levels between different genotypes. Lower-case letters indicate the statistically significant ($P < 0.05$) differences between genotypes.
(d) Proportion 4MO-I3M GSL in the total amount of indole-GSLs in WT, *pp2a-b′γ* and *pp2a-b′γ 35S::PP2A-B′γ* complementation line in different measurements. One-way ANOVA followed by Tukey's pairwise comparisons was used to analyse the 4MO-I3M GSL/indole-GSL ratios between different genotypes. Lower-case letters indicate the statistically significant ($P < 0.05$) differences between genotypes.
(e) Simplified scheme depicting the biosynthesis of methoxylated indole GSLs from tryptophan (Trp). Indole-3-acetaldoxime (IAOx) provides a common precursor for the biosynthesis of camalexin and indole GSLs. The abundant intermediate I3M can be hydroxylated by two different cytochrome p450 family enzymes (CYP81F2 and CYP81F4) and the hydroxylated reaction products are subjects for methylation by IGMT activity, yielding specifically methoxylated 4MO-I3M and 1MO-I3M (Pfalz *et al.*, 2011).

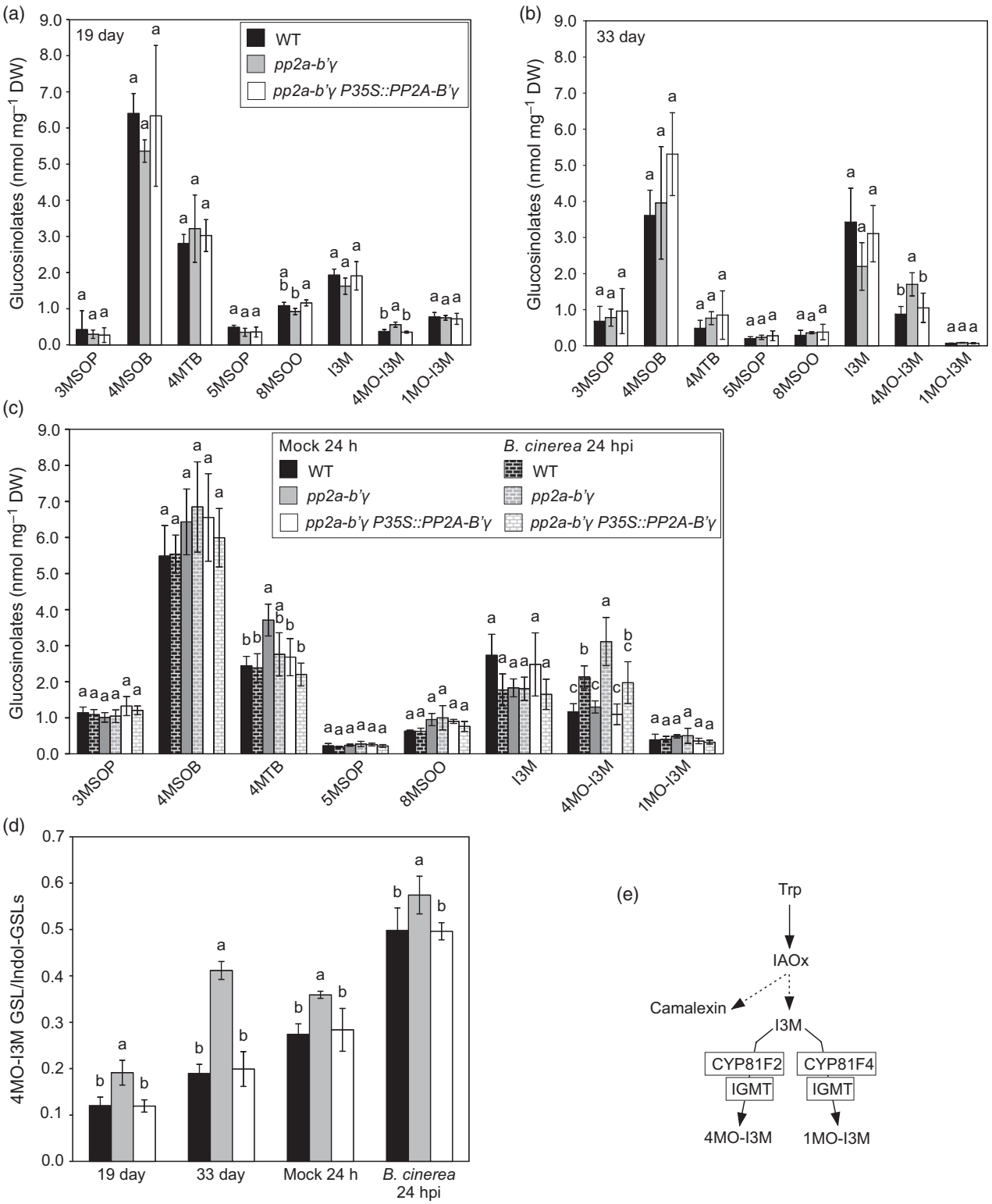

threonine content, which is known to be modulated by SAM (Curien *et al.*, 2009; Amir, 2010). Also, the SAM/SAH ratio (methylation index) of *pp2a-b'γ* was increased compared with the wild type and the complementation line, which is indicative of an improved cellular potential for methylation reactions in the mutant line (Figure 3a).

PP2A-B′γ modulates the abundance of SAHH1- and CIMS1-containing oligomers

Next we took a proteomics approach to decipher potential phosphorylation, protein interactions and metabolic connections among components of the activated methyl cycle and other cellular pathways. By means of clear native (CN)-PAGE fractionation and subsequent Western blotting with anti-SAHH antibody, it was possible to visualize six oligomeric complexes of SAHH (Figure 4a). Structural studies have shown that SAHH is dimeric in plants (Brzezinski *et al.*, 2012), whereas in prokaryotes and mammals it functions as a tetramer (Reddy *et al.*, 2008; Ishihara *et al.*, 2010). Based on the molecular weight (MW) markers, the two smallest SAHH complexes represented a free monomer and a dimer (complexes 5 and 6 in Figure 4a). The other four oligomers ranged between 140 and 440 kDa, with oligomer number 4 being the most intense one and present in elevated levels in *pp2a-b′γ* leaves compared with the wild type (Figure 4a). CIMS, which catalyses the step following SAHH in the activated methyl cycle, has been reported to function as a 84-kDa monomer (Ferrer *et al.*, 2004) but was found to migrate between the 140- and 232-kDa molecular markers as an oligomeric high-MW complex, which showed decreased abundance in *pp2a-b′γ* compared with the wild type (Figure 4b).

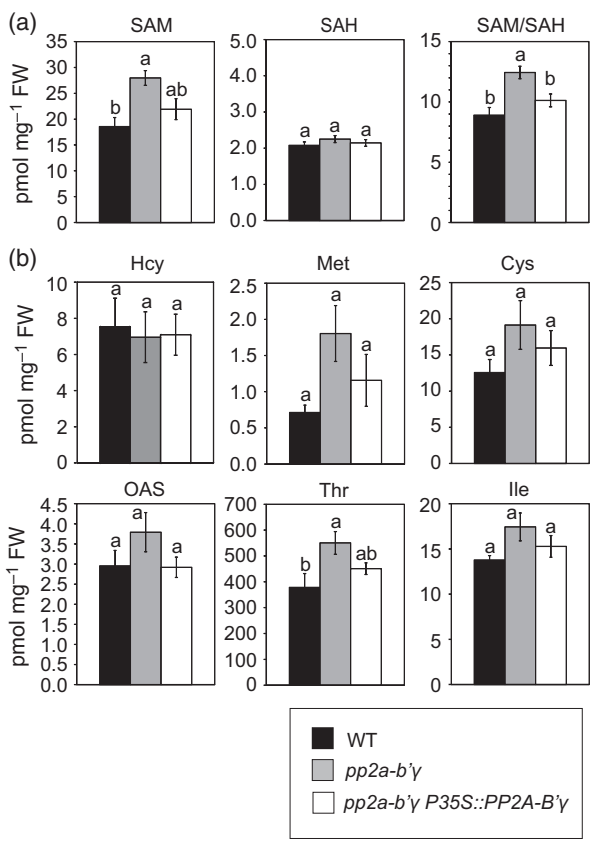

Figure 3. Content of activated methyl cycle intermediates and selected amino acids in *pp2a-b′γ* and wild-type (WT) plants.
(a) *S*-adenosyl-L-methionine (SAM) and *S*-adenosyl-homocysteine (SAH) content and SAM/SAH ratio in 4-week old WT, *pp2a-b′γ* and *pp2a-b′γ 35S::PP2A-B′γ* complementation lines. Results are means (n = 7–8)
(b) HCy, Met, Cys, OAS, Thr and Ile content of WT, *pp2a-b′γ* and *pp2a-b′γ 35S::PP2A-B′γ*. For Met, OAS, Thr and Ile, results are means (n = 7–8). For the thiols Hcy and Cys, results are means (n = 5–6). HCy, homocysteine; Met, methionine; Cys, cysteine, OAS, *O*-acetylserine; Thr, threonine; Ile, isoleucine. One-way ANOVA followed by Tukey's pairwise comparisons was used to analyze the metabolite levels between different genotypes. Lowercase letters indicate the statistically significant ($P < 0.05$) differences between genotypes.

To assess the oligomeric compositions of SAHH- and CIMS-containing complexes, we used a gel-based 3D approach, which as a combination of 1D CN-PAGE, 2D SDS-PAGE and 3D SDS-PAGE had previously proven instrumental in identifying the protein components of mitochondrial complex I in Arabidopsis (Peters *et al.*, 2013). We substituted 2D SDS-PAGE with 2D CN-PAGE to better separate the SAHH and CIMS oligomers of interest. The total soluble leaf extract of *pp2a-b′γ* was first separated on CN-PAGE (in a 7.5–15% gradient acrylamide gel), and the area corresponding to the main SAHH complex was excised and placed vertically on top of a second CN-PAGE, where it was separated with a different acrylamide gradient (8–9%). Finally, from this gel, the entire vertical lane was cut out, solubilized and separated as a horizontal gel strip in SDS-PAGE (Figure 4c).

The spots visible in the third dimension were excised for MS analysis of protein identity and phosphorylation. The abundant spot co-migrating with SAHH1 turned out to be carbonic anhydrase 1 (CA1; previously identified as the chloroplastic salicylic acid-binding protein 1, SABP3) (Slaymaker *et al.*, 2002). CIMS1 in turn associated with methylenetetrahydrofolate reductase 1 (MTHFR1) (Figure 4d, Table 2), which provides the methyl donor required for CIMS activity within the activated methyl cycle. These proteins additionally co-migrated with the myrosinase TGG1 and heat shock protein 70 (HSP70) (Figure 4d, Table 2). In addition to SAHH1 phosphorylation (Trotta *et al.*, 2011; Li *et al.*, 2014; Table 2), CIMS1 was identified as a phosphoprotein with two phosphorylation sites (Table 2). SAHH1 and CIMS1 could hence represent targets for PP2A-dependent regulation.

Finally, BiFC analysis was used to assess possible binary interactions among the identified methionine metabolism-related components. YFP fluorescence, indicative of protein interaction, was observed between PP2A-B′γ and SAHH1 and CIMS1, but not with TGG1, which, however, interacted with itself, indicative of dimer formation in the transient assay (Fig. 5). SAHH1 was found to interact with CIMS1. SAHH also interacted with itself, which is in line with its reported dimeric holoenzyme in plants (Brzezinski *et al.*, 2012). Even though TGG1 and SAHH have been reported to co-exist in trichomes (Wienkoop *et al.*, 2004; Frerigmann *et al.*, 2012) and sulfur-rich S-cells (Koroleva and Cramer, 2011), no BiFC interaction between SAHH1

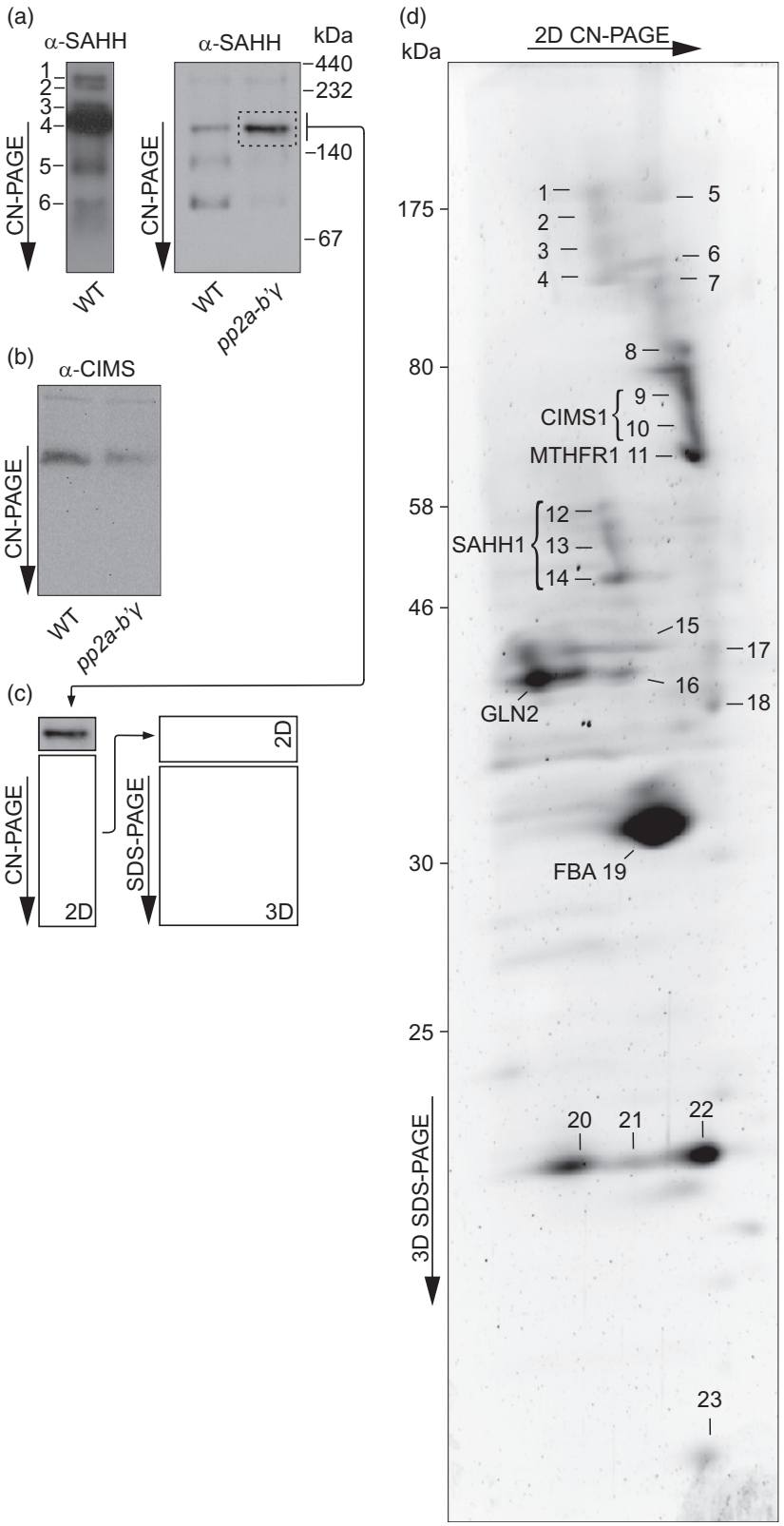

Figure 4. Analysis of *S*-adenosylhomocysteine hydrolase 1 (SAHH1)- and cobalamine-independent methionine synthase 1 (CIMS1)-containing protein complexes in Arabidopsis.

(a) Six SAHH-containing protein complexes as detected by α-SAHH antibody in total soluble protein extract of 4-week old wild type (WT) and *pp2a-b′γ* separated on clear native PAGE. Complex 5 corresponds to the molecular mass of SAHH1 homodimer (MW = 106 kDa). The first panel is over-exposed for visualization of the high-MW complexes.

(b) Clear native PAGE of total soluble protein samples of 4-week old WT and *pp2a-b′γ* as detected by α-CIMS antibody.

(c) Scheme depicting the gel-based 3D approach. Total soluble extract of *pp2a-b′γ* was first separated by CN-PAGE, and the area corresponding to the area around the main SAHH complex was excised and placed vertically on top of a second CN-PAGE gel, where it was separated with a different acrylamide gradient. From this gel, the entire vertical lane was cut out, solubilized and separated as a horizontal gel strip in SDS-PAGE as shown in (d).

(d) 3D CN-PAGE separation of the SAHH- and CIMS-containing complexes. Protein spots indicated by the numbers 1–23 were analyzed by MS/MS and are presented in Table 2. MTHFR1, methylenetetrahydrofolate reductase 1.

Table 2 Proteins and phosphopeptides identified in the soluble leaf extract of *pp2a-b′γ* by 3D clear native PAGE and data-dependent acquisition by nanoscale liquid chromatography/electrospray ionization tandem mass spectrometry. The protein spots analysed are as indicated in Figure 4(d). The second and third hits in the identification are indicated if the score, peptide spectrum matches (PSM) or the number of peptides was more than half of that of the first hit in the analysed spot

Spot	Uniprot ID	Gene	Identifier	Full name	Score	PSM/ peptides	Phosphopeptides
1	Q9ZNZ7	*At5g04140*	FD-GOGAT	Ferredoxin-dependent glutamate synthase 1	1254	35/35	
	Q94B78	*At4g33010*	ATGLDP1	Glycine decarboxylase P-protein 1	742	25/21	
2	Q94B78	*At4g33010*	ATGLDP1	Glycine decarboxylase P-protein 1	1015	26/20	IKC(p)SDAHAIADAASK
3	Q94B78	*At4g33010*	ATGLDP1	Glycine decarboxylase P-Protein 1	987	28/23	
	Q9LF37	*At5g15450*	ATCLPB3	Casein lytic proteinase B3	922	21/21	
	Q9ASR1	*At1g56070*	LOS1	Low expression of osmotically responsive genes 1	703	18/18	
4	Q94B78	*At4g33010*	ATGLDP1	Glycine decarboxylase P-protein 1	590	22/15	
	Q9ASR1	*At1g56070*	LOS1	Low expression of osmotically responsive genes 1	401	11/10	
	Q9SRV5	*At3g03780*	ATMS2	Methionine synthase 2	357	15/14	
5	Q9ZNZ7	*At5g04140*	FD-GOGAT	Ferredoxin-dependent glutamate synthase 1	1602	41/36	GSD(p)SANLDSAAEIMIR
6	Q9ZNZ7-2	*At5g04140*	FD-GOGAT	Ferredoxin-dependent glutamate synthase 1	556	8/7	GNADIIQI(p) SGHDGGTGASPISSIK
	O50008	*At5g17920*	ATCIMS	Cobalamin-independent methionine synthase	499	15/14	
7	O50008	*At5g17920*	ATCIMS	Cobalamin-independent methionine synthase	683	19/14	
	Q9FI56	*At5g50920*	CLPC1	CLPC homolog 1	656	18/18	
	Q56WK6	*At1g72150*	PATL1	Patellin 1	649	16/16	
8	Q9FI56	*At5g50920*	CLPC1	CLPC homolog 1	1120	31/30	
	P22953	*At5g02500*	HSP70-1	Heat shock cognate protein 70-1	697	16/16	
	O50008	*At5g17920*	ATCIMS	Cobalamin-independent methionine synthase	658	17/13	
9	O50008	*At5g17920*	ATCIMS	Cobalamin-independent methionine synthase	1085	35/20	IP(p)SSEEIADRVNK KV(p)SEEDYVK
	P37702	*At5g26000*	TGG1	Thioglucoside glucohydrolase 1	740	24/12	
	P22953	*At5g02500*	HSP70-1	Heat shock cognate protein 70-1	684	16/14	
10	P37702	*At5g26000*	TGG1	Thioglucoside glucohydrolase 1	750	31/10	
	O50008	*At5g17920*	ATCIMS	Cobalamin-independent methionine synthase	434	21/10	
11	P37702	*At5g26000*	TGG1	Thioglucoside glucohydrolase 1	1506	50/22	
	P34795	*At5g42740*	PGIC	Glucose-6-phosphate isomerase	675	15/15	
	Q9SE60	*At3g59970*	MTHFR1	Methylenetetrahydrofolate reductase 1	501	15/15	
12	O23255	*At4g13940*	SAHH1	*S*-adenosyl-L-homocysteine hydrolase 1	357	11/11	
13	Q9M5K3	*At1g48030*	MTLPD1	Mitochondrial lipoamide dehydrogenase 1	816	19/19	
	O23255	*At4g13940*	SAHH1	*S*-adenosyl-L-homocysteine hydrolase 1	705	20/14	
	Q56YU0	*At3g24503*	ADH1	Aldehyde dehydrogenase 1A	514	10/10	
14	Q56YU0	*At3g24503*	ADH1	Aldehyde dehydrogenase 1A	800	17/16	
	O23255	*At4g13940*	SAHH1	*S*-adenosyl-L-homocysteine hydrolase 1	727	27/19	LVGV(p)SEETTTGVKR
	P55229	*At5g19220*	AGPL1	ADP glucose pyrophosphorylase large subunit 1	686	17/17	
15	Q9LR30	*At1g23310*	GGAT1	Glutamate:glyoxylate aminotransferase 1	738	19/16	
16	Q43127	*At5g35630*	GLN2	Glutamine synthetase 2	530	16/13	HKEHI(p)SAYGEGNER
	P25857	*At1g42970*	GAPB	Glyceraldehyde-3-phosphate dehydrogenase B subunit	437	11/11	
17	P46248	*At4g31990*	ASP5	Aspartate aminotransferase 5	566	14/14	
	O82662	*At2g20420*	SUCB	Succinyl-CoA ligase [ADP-forming] subunit beta	466	13/12	

(continued)

Table 2. (continued)

Spot	Uniprot ID	Gene	Identifier	Full name	Score	PSM/ peptides	Phosphopeptides
18	P46248	*At4g31990*	ASP5	Aspartate aminotransferase 5	665	22/17	VA(p)TIQGLSGTGSLR
	P25857	*At1g42970*	GAPB	Glyceraldehyde-3-phosphate dehydrogenase B subunit	570	17/14	
	Q9LFA3	*At3g52880*	MDAR1	Monodehydroascorbate reductase 1	505	13/12	
19	Q944G9	*At4g38970*	FBA2	Fructose-bisphosphate aldolase 2	1781	107/28	ANsLAQLGKYTGEGESEEAK
20	P27140	*At3g01500*	CA1, SAB3	Beta carbonic anhydrase 1	2026	63/15	YE(p)TNPALYGELAK
							(p)YMVFACSDSR
21	P27140	*At3g01500*	CA1, SAB3	Beta carbonic anhydrase 1	429	12/11	
22	Q42029-2	*At1g06680*	PSBP-1	Oxygen-evolving enhancer protein 2	594	41/9	(p)
				TADGDEGGKHQLITATVNGGK		P27140	*At3g01500*
CA1,	SAB3	Beta carbonic		anhydrase 1	535	13/10	
23	P39207	*At4g09320*	ATNDK1	Nucleoside diphosphate kinase 1	581	20/9	IIGA(p)TNPAASEPGTIR (p)SFAEKHYEDLSSK

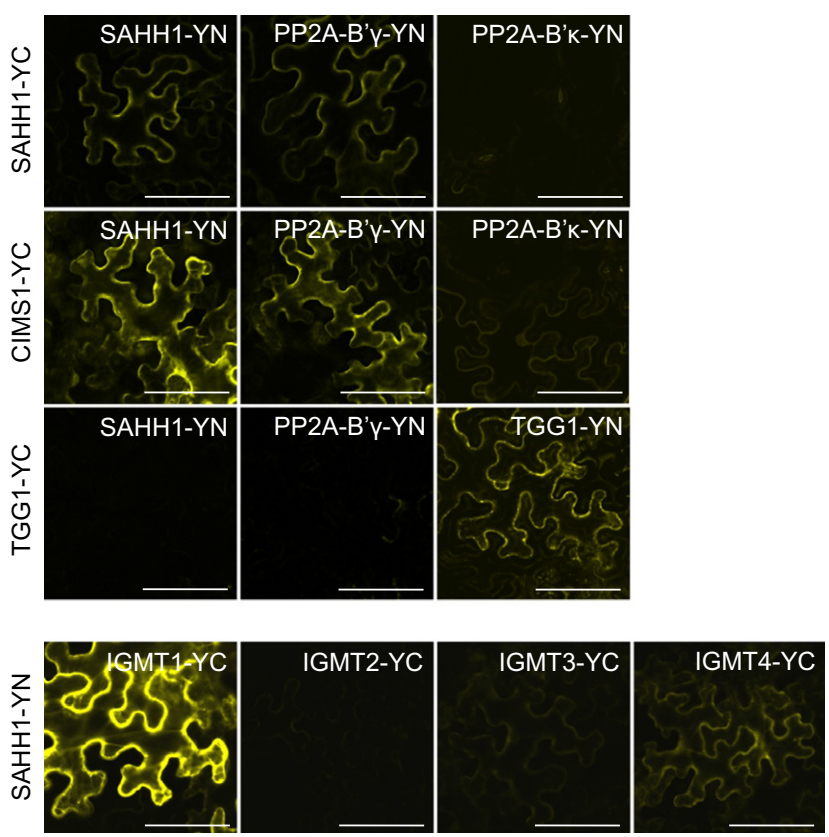

Figure 5. Bimolecular fluorescence complementation assay in *Nicotiana benthamiana* leaves expressing SAHH1-YN, PP2A-B′γ-YN, PP2AB′κ or TGG1-YN and SAHH1-YC, CIMS1-YC, TGG1-YC or IGMT1-YC fusion proteins under the 35S promoter.
SAHH1, *S*-adenosylhomocysteine hydrolase 1; PP2A-B′γ, protein phosphatase 2A regulatory subunit B′γ; TGG1, beta-thioglucoside glucosidase 1; CIMS1, cobalamine-independent methionine synthase 1; IGMT1, indole glucosinolate methyltransferase 1. Scale bars correspond to 100 μm.

and TGG1 could be observed. Finally, BiFC analysis also suggested a physical interaction between SAHH1 and the IGMTs (Figure 5). Strong fluorescence was detected when SAHH1 was co-expressed with IGMT1, while moderate fluorescence was observed with IGMT4. Only weak fluorescence was detected with IGMT2 and -3. Immunoblot analysis confirmed that all IGMT isoforms were expressed in the *N. benthamiana* leaves (Fig. S1).

DISCUSSION

PP2A-B′γ is required to control the biosynthesis of specifically modified indole glucosinolates

The GSLs of cruciferous plants comprise a major group of structurally diverse secondary compounds involved in several aspects of plant metabolism, but the underlying mechanisms of their biological roles are not yet known. A substantial research effort has led to the identification of the enzymatic machineries involved in the biosynthesis of the core structure, specific modifications, degradation and transport of GSLs (Sønderby *et al.*, 2010; Nour-Eldin *et al.*, 2012). Several recent studies have indicated transcriptional regulation as a key level in the regulation of these processes, whereas post-translational regulatory actions that specifically control the decoration and activity of indole GSLs have not been reported. Here we demonstrate that PP2A-B′γ negatively regulates the methoxylation of hydroxylated indole GSLs and the formation of 4MO-I3M in particular. Moreover, PP2A-B′γ controls the supramolecular enzymatic machineries functionally linked with the activated methyl cycle and *trans*-methylation capacity in Arabidopsis leaves (Figure 6).

The conversion of I3M to 4MO-I3M yields an ecologically important modified GSL that specifically acts as a repellant for microbial pathogens and aphids, but at the same time influences oviposition preferences of crucifer-specialist lepidopterans, both as an intact and degraded molecule (Kroymann, 2011). Furthermore, enzymatic degradation of 4MO-I3M by the myrosinase PEN2 promotes intracellular signaling effects that execute inducible defenses against non-host fungal and bacterial invasion (Bednarek *et al.*, 2009; Clay *et al.*, 2009). The cytochrome P450 family hydroxylases and the IGMTs catalyzing the two-step conversion of I3M to 4MO-I3M are highly conserved in evolutionarily distant cruciferous species, as are their biological roles (Fahey *et al.*, 2001; Bednarek *et al.*, 2011). However, the ratios and relative concentrations of I3M and 4MO-I3M with respect to total GSL content varies considerably in all Brassicaceae family species studied to date, reflecting the importance of these particular molecular species in the evolution of specific plant–insect interactions in defined ecological niches (Bednarek *et al.*, 2011).

Studies have identified key transcriptional regulators, such as altered tryptophan regulation 1/MYB34 (Bender

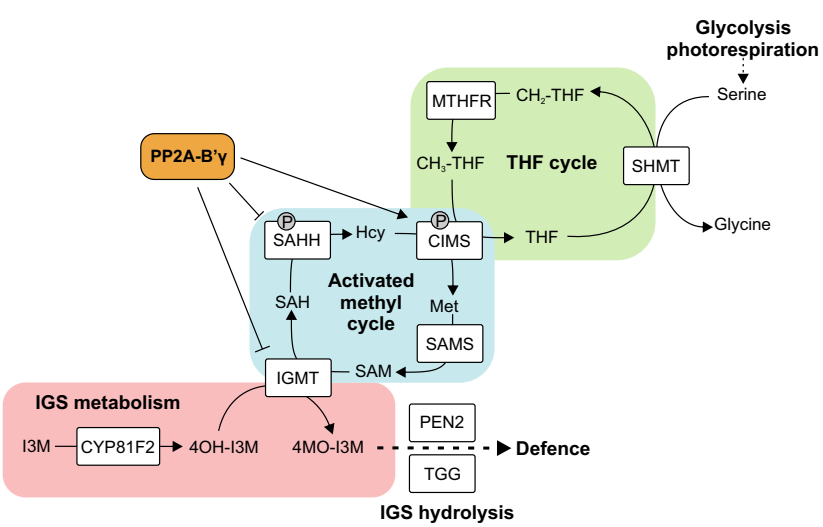

Figure 6. Schematic representation of protein phosphatase 2A regulatory subunit B′γ (PP2A-B′γ) as a regulator of methionine metabolism in Arabidopsis.
Indole glucosinolates (IGS) of cruciferous plants are thiol-rich secondary compounds, whose degradation by penetration 2 (PEN2) and beta-thioglucoside glucosidase (TGG) myrosinases yield breakdown products with diverse roles in plant-biotic interactions. PP2A-B′γ interacts with indole glucosinolate methyltransferases 1 and 4 (IGMT1 and IGMT4) and is required to control the formation of 4-methoxy-indol-3-yl-methyl (4MO-I3M, 4-methoxyglucobrassicin) in Arabidopsis leaves. The IGMT-driven *trans*-methylation reaction is tightly connected with the activated methyl cycle to ensure efficient detoxification of the inhibitory reaction product *S*-adenosyl homocysteine (SAH) by *S*-adenosylhomocysteine hydrolase (SAHH). PP2A-B′γ negatively regulates the abundance of SAHH1 in specific oligomeric complexes, but is required to maintain the abundance of cobalamine-independent methionine synthase (CIMS) oligomers to coordinate balanced regeneration of methionine (Met) and the universal methyl donor *S*-adenosylmethionine (SAM). CIMS is functionally tightly linked to methylenetetrahydrofolate reductase (MTHFR), which provides the methyl donor required for CIMS activity within the activated methyl cycle. SAMS, SAM synthase; SHMT, serine hydroxymethyltransferase; HCy, homocysteine; THF, tetrahydrofolate; CH_2-THF, methylene-tetrahydrofolate; CH_3-THF, methyl-tetrahydrofolate.

and Fink, 1998; Celenza *et al.*, 2005), high indole glucosinolate 1/MYB51 (Gigolashvili *et al.*, 2007) and IQ-domain 1 (IQD1) (Levy *et al.*, 2005) as global activators of indole GSL biosynthesis. Transcriptional regulation may, however, also affect the variation in modified indole GSL content (Schlaeppi *et al.*, 2010; Frerigmann *et al.*, 2016). This was demonstrated by the identification of *cis*- and *trans*-acting factors that control the transcript abundance for CYP81F2, the key enzyme catalysing the hydroxylation of I3M to 4OH-I3M, a barely detectable intermediate that provides the substrate for IGMT activity (Pfalz *et al.*, 2009; Schlaeppi *et al.*, 2010).

Of the indole GSL methyltransferases, IGMT1–IGMT3 become transcriptionally activated upon infestation by green peach aphid (De Vos and Jander, 2009), whereas IGMT1 and IGMT2 showed increased transcript abundance in *B. cinerea*-infected leaves (Xu *et al.*, 2016). IGMT4, in contrast, appears to be constitutively expressed at a level that is detectable by LC-MS/MS in non-stressed Arabidopsis leaves, whereas IGMT1–IGMT3 could not be unequivocally detected (Table 1). Our findings indicate that the activity of IGMTs and the formation of 4MO-I3M is post-translationally negatively regulated by PP2A-B′γ in wild-type Arabidopsis leaves (Figures 1, 2 and 6). Even though the MS/MS analysis did not detect IGMT phosphopeptides (Table 1), PP2A-B′γ-dependent regulation by reversible protein phosphorylation may still provide a mechanism for controlling the production of 4MO-I3M. One possibility is that PP2A-B′γ, IGMT and SAHH1 come into contact through a transient interaction, where SAHH1 rather than the IGMT is the substrate for regulation by PP2A. Protein interaction between IGMT4 and SAHH1 is supported by positive BiFC signals (Figure 5), and SAHH is also known to interact with other methyltransferases, such as the Arabidopsis mRNA cap methyl-transferase (CMT), presumably to ensure efficient *trans*-methylation reactions (Lee *et al.*, 2012). Understanding the molecular machineries that allocate GSL intermediates to their final products is one of the key outstanding questions in GSL research (Sønderby *et al.*, 2010). It is therefore of interest that PP2A-B′γ modulates the production of a specific modified indole GSL, and may therefore offer previously unrecognized perspectives for metabolic engineering.

PP2A-B′γ controls a system of cross-communicating metabolic cycles in methionine metabolism

The biosynthesis of GSLs is tightly integrated with amino acid metabolism, a theme increasingly associated with the resistance of plants to biotic stress factors (Sønderby *et al.*, 2010; Fan *et al.*, 2011; Stuttmann *et al.*, 2011; Trotta *et al.*, 2011; Alvarez *et al.*, 2012). Within these regulatory networks, PP2A-B′γ exerts a control over methionine metabolism, and particularly SAHH1 and CIMS1 in the activated methyl cycle in the cytoplasm (Figure 6). The importance of SAHH1 in the maintenance of methyl group homeostasis during basic metabolism has been evidenced by the drastic phenotypic properties of Arabidopsis *sahh1* loss-of-function mutants, which undergo significant alterations in gene expression, metabolic profiles and developmental programs, and display severe dwarfism and low fertility (Rocha *et al.*, 2005; Ouyang *et al.*, 2012). The genes differentially expressed in young *sahh1* mutant seedlings display reduced transcript abundance for seven methyltransferases, and these include IGMT1 and IGMT2 (Ouyang *et al.*, 2012). This observation suggests that deficiencies in the functional state of the methyl cycle can be readily signaled to re-adjust the capacity to methylate indole GSLs.

The ability to increase cellular *trans*-methylation capacity and the recycling of methionine upon activation of stress-induced biosynthetic processes is also essential for cellular vitality. This has been evidenced as transcriptional and post-translational upregulation of the methyl cycle enzymes as well as the increased abundance of methyl cycle intermediates upon activation of plant defenses towards oomycetes, necrotrophic fungi and bacterial pathogens (Figure 4) (Elmore *et al.*, 2012; Arasimowicz-Jelonek *et al.*, 2013; Winterberg *et al.*, 2014; Li *et al.*, 2015). The centrality of *trans*-methylation reactions in plant immunity is further reflected by the identification of SAHH and SAMS as targets for manipulation by pathogen effectors (Ivanov *et al.*, 2016).

Here we have identified both SAHH1 and CIMS1 as phosphoproteins, the abundance of which in oligomeric protein complexes is modulated by PP2A-B′γ (Figure 4, Table 2). In non-stress-exposed wild-type Arabidopsis leaves, PP2A-B′γ negatively regulates the biosynthesis of defense-active secondary compounds, hinders the accumulation of SAHH1 into a specific highly abundant oligomeric complex, maintains the abundance of CIMS oligomers and keeps the level of SAM in balance (Figures 2–4 and 6) (Li *et al.*, 2014). CIMS was found to associate with MTHFR, suggesting an oligomeric protein complex that directly connects the activated methyl cycle with folate metabolism (Figures 4 and 6).

Folate-dependent metabolism is a complex network in which one-carbon units are used for key biosynthetic and regulatory functions, and strict control of folate homeostasis is therefore essential in sustaining the demand for C1-units. Folate depletion, induced by antifolate drugs or by gene disruption, results in shuttling of C1-units to the synthesis of nucleotides at the expense of methylation reactions (Loizeau *et al.*, 2008). The impairment of the methyl cycle thereafter hinders essential metabolic pathways, such as chlorophyll biosynthesis (Van Wilder *et al.*, 2009), and prevents accurate epigenetic regulation through methylation of DNA and histones (Zhang *et al.*, 2012; Zhou *et al.*, 2013). Also, it is known that Arabidopsis MTHFR

performs a reversible reaction and is not feedback inhibited by SAM (Roje *et al.*, 1999). In Arabidopsis, CIMS is monomeric (Ferrer *et al.*, 2004), while MTHFR forms homodimers (Roje *et al.*, 1999). The sum of their corresponding MWs (84 and 132 kDa, respectively) is consistent with the apparent MW of the oligomer identified by 3D-PAGE (Figure 4, Table 2). Compartmentalization within a multienzyme complex presumably ensures an efficient supply of the methyl donor for formation of methionine by CIMS activity (Figure 6). Given the multifaceted functions of cellular *trans*-methylation reactions, it is plausible that methionine cycle components undergo modulations in their oligomeric protein compositions and form complexes with enzymes functionally connected with diverse cellular pathways (Moffatt *et al.*, 2002; Rocha *et al.*, 2005; Loizeau *et al.*, 2008; Ouyang *et al.*, 2012).

PP2A-B′γ-dependent modulations in the activated methyl cycle are associated with enhanced pathogenesis responses (Figures 2 and 4) (Trotta *et al.*, 2011; Li *et al.*, 2014). In addition to the impact on the production of 4MO-I3M (Figure 2), PP2A-B′γ is required to control salicylic acid-dependent defense responses and the associated formation of scopoletin, but the molecular mechanisms governing this SAM-consuming biosynthetic pathway are not well established (Li *et al.*, 2014). DNA, in contrast, has been reported to undergo hypomethylation upon activation of defense responses, presumably to facilitate the expression of immunity-related genes by mediating decondensation of the chromatin structure (Pavet *et al.*, 2006; Trotta *et al.*, 2011). Evidently, tight regulation of the methyl cycle and its specific enzymatic steps is vital to meet the needs of distinct metabolic and regulatory reactions occurring in different cellular compartments.

Taken together, we propose that PP2A-B′γ controls the methylation step in the production of the specifically decorated indole GSL 4MO-I3M. This PP2A-B′γ-dependent regulatory action is tightly connected with a downstream system of cross-communicating metabolic cycles that maintain *trans*-methylation capacity and methionine metabolism in plant cells (Figure 6). The involvement of PP2A-B′γ in the coordination of methyl utilization highlights the involvement of post-translational regulation in metabolic networks, and is an additional important consideration in future efforts to engineer biofortified crops

EXPERIMENTAL PROCEDURES

Plant material and growth conditions

Arabidopsis thaliana ecotype Columbia wild type and mutants were grown under 130 μmol photons m^{-2} sec^{-1}, 22°C and 50% humidity at an 8-h light period. *Botrytis cinerea* was grown on potato dextrose agar plates. For infection, the plants were grown for 4 weeks at 23/18°C and 65/75% humidity under an 8/16 h (day/night) photoperiod, and infected by spraying with a 1×10^6 *B. cinerea* spore suspension in 0.5× potato dextrose broth (PDB) and covered to maintain under 100% humidity. Mock-treated plants were sprayed with 0.5× PDB and treated in parallel to the infected plants. Samples were collected 24 h post-infection and immediately frozen in liquid nitrogen. Homozygote *pp2a-b′γ* (SALK_039172 for AT4G15415) and a *pp2a-b′γ* line complemented by 35S-driven expression of the *PP2A-B′γ* gene were previously generated and genotypically confirmed (Trotta *et al.*, 2011; Rasool *et al.*, 2014). Experiments were conducted with 3- or 4-week-old plants, as indicated in the text.

Yeast two-hybrid screening

Yeast two-hybrid screening was conducted with HybridHunter (Invitrogen, http://www.invitrogen.com) using the L40 yeast strain and LexA DBD fusion of PP2A-B′γ in pHybLex as bait against a cDNA library enriched for stress-related factors, as described in Jaspers *et al.* (2009). A hundred thousand (10^5) colony-forming units of tryptophan auxotrophic yeast were placed on –His selection supplemented with 10 mM 3-aminotriazole (3AT; Sigma-Aldrich, http://www.sigmaaldrich.com) to remove autoactivation. Colonies were picked after 4 days of growth at 28°C and tested for β-galactosidase activity according to the HybridHunter manual. Putative interaction partners in the pYESTrp2 library plasmid were identified by sequencing.

BiFC analysis

All constructs for BiFC analyses were introduced into pGPTVII backbone vectors and verified by sequencing (Walter *et al.*, 2004; Waadt and Kudla, 2008). Complete protein-coding regions were amplified by PCR and fused to C-terminal fragment (SPYCE) or N-terminal fragment (SPYNE) of YFP using the primers indicated in Table S4. *Agrobacterium tumefaciens* strain GV3101/PMP90 carrying the fluorescent fusion constructs were infiltrated into *N. benthamiana* leaves according to Waadt and Kudla (2008). The YFP fluorescence was imaged with confocal laser scanning microscopes Zeiss LSM780 with an excitation at 514 nm and detection at 519–621 nm (Figures 1 and 5, lower panel) and Zeiss LSM510 META with excitation at 514 nm and detection at 535–590 nm or 530–600 nm (Figure 5, upper panel). Maximal projections of the sequential confocal images were created with Zeiss Zen 2.1 software version 11.0.0.190 (http://www.zeiss.com).

Proteomic analysis

Extraction of total soluble leaf extracts was performed in the presence of protease (Complete-Mini; Roche, https://www.sigmaaldrich.com) and phosphatase (PhosSTOP; Roche) inhibitors using the methods described by Kangasjärvi *et al.* (2008). For identification of proteins from 1D SDS gels, proteins were separated on 12% polyacrylamide gel, after which the gel was Coomassie-stained and bands of appropriate size were cut out and subjected to in-gel trypsin digestion; protein identification was by data-dependent nLC/ESI-MS/MS using Q-Exactive (Thermo Scientific, https://www.thermofisher.com) as in Li *et al.* (2014). The MS/MS spectra were analyzed against TAIR10 as in Trotta *et al.* (2016). Results were analyzed through Proteome Discover v.1.4 (Thermo Scientific) allowing Met oxidation, Cys carboamidomethylation and Ser/Thr and Tyr phosphorylation as possible modifications.

For analysis by CN-PAGE, total soluble leaf extracts corresponding to 5 μg of proteins were loaded for subsequent immunoblotting with antibodies against SAHH and CIMS as in Trotta *et al.* (2011). For analysis by a 3D approach, 200 μg of total soluble extract was first separated on 5–15% gradient CN-PAGE and the area corresponding to approximately 140–240 kDa oligomeric

complexes was excised and placed vertically on top of a second CN-PAGE, where it was separated with a different (8–9%) acrylamide gradient. From this second native gel, the entire vertical lane was cut out, solubilized and separated as a horizontal gel strip in 12% SDS-PAGE. After imaging the gels with SYPRO Ruby (Invitrogen), mass spectrometry was performed as described by Li *et al.* (2014) using a LC-ESI-MS/MS system (QTOF Elite; AB Sciex, http://www.absciex.com/). The MS/MS spectra were analyzed with an in-house installation of Mascot (http://www.matrixscience.com), with searches restricted to the Uniprot Arabidopsis database.

To monitor the expression of BiFC fusion proteins, *N. benthamiana* leaves were ground in liquid nitrogen and mixed with extraction buffer [10 mM HEPES-KOH pH 7.5, 10 mM $MgCl_2$, 20 mM DTT supplemented with protease (Complete-Mini; Roche) and phosphatase (PhosSTOP; Roche) inhibitors]. Samples were centrifuged at 18 000 ***g*** for 15 min and the soluble fracture was taken for immunoblot analysis. Proteins were separated on 10% SDS-PAGE. Anti-c-myc (9E10) monoclonal antibody (Covance Research Products Inc., cat. no. MMS-150R) was used to identify YN fusion proteins and anti-HA (16B12) monoclonal antibody (Covance Research Products Inc., cat. no. MMS-101R) for YC fusion proteins.

Analysis of metabolites

For analysis of SAM, SAH, soluble thiols and amino acids, approximately 100 mg of leaf material was weighed, ground to a fine powder in liquid nitrogen and extracted once by incubation for 15 min at room temperature (20°C) with 100 μl of 50% (v/v) acetonitrile and 25 mM HCl (analytical grade), and finally centrifuged for 15 min at 12 000 ***g*** at 4°C. All supernatant was collected, the exact volume was determined and aliquots were stored at −20°C.

The method for analysis of SAM and SAH was adopted from Castro *et al.* (2002) and performed as described in Loizeau *et al.* (2007). Amino acids were measured by pre-column derivatization with *o*-phthaldialdehyde followed by HPLC using a Hypersil C18, 150 mm × 4.6 mm ID, 3-μm column (Knauer GmbH, http://www.knauer.net/) as described by Kreft *et al.* (2003). Thiols were derivatized by monobromobimane as described by Fahey and Newton (1987) and subjected to HPLC analysis using an Atlantis dC18, 250 mm × 4.6 mm ID, 5 μm column (Waters, http://www.waters.com/) as described by Loizeau *et al.* (2007). For each analysis, mixed standards (Sigma) treated exactly as the sample supernatants were used as a reference for quantification.

The GSL contents in non-stress-exposed and 4-week-old *B. cinerea*-infected plants were determined as previously described (Mikkelsen and Halkier, 2003).

Statistical analyses

The numerical data were subjected to statistical analysis using one-way ANOVA with statistical significance at the level of $P < 0.05$, followed by Tuckey's pairwise comparisons.

ACKNOWLEDGEMENTS

This work was supported by the Academy of Finland (271832, 273870 and 251397, 256073, 283254 to KO) and the University of Turku Doctoral Program in Molecular Life Sciences. EG is supported by a DFG Heisenberg Fellowship (GL346/5) and the TUM Junior Fellow Fund. JP is supported by a FPU Fellowship (AP2010-5857, Ministry of Education, Spain). BM is supported by a Discovery Grant from the Natural Sciences and Engineering Research Council of Canada. KV is a member of the University of Helsinki Doctoral Program in Plant Science (DPPS). We acknowledge support from the Finnish Microarray and Sequencing Centre and Biocenter Finland Proteomics and Metabolomics infrastructures to conduct this work. AB Sciex are acknowledged for their support with Protein Pilot. The Salk Institute Genomic Analysis Laboratory is acknowledged for providing the sequence-indexed Arabidopsis T-DNA insertion mutants. Confocal imaging was performed at the Cell Imaging Core, Turku Centre for Biotechnology, University of Turku and Åbo Akademi University. Zsofia Winter and Ella Muhli are acknowledged for excellent technical assistance. The authors declare no conflict of interest.

SUPPORTING INFORMATION

Additional Supporting Information may be found in the online version of this article.

Figure S1. Immunoblot analysis of fusion protein expression in bimolecular fluorescence complementation experiments in Figures 1(b) and 5.

Figure S2. Visual phenotypes of 19- and 33-day-old wild type, *pp2a-b′γ* and *pp2a-b′γ 35S::PP2A-B′γ* Arabidopsis plants prior to the glucosinolate analysis.

Table S1. Proteins with an approximate molecular mass of 40 kDa identified from total soluble extracts, listed according to the sum of peptide spectrum matches detected in wild-type, *pp2a-b′γ* and *pp2a-b′γ P35S::PP2A-B′γ* samples in two biological replicates.

Table S2. Proteins migrating above the 40-kDa gel band in wild-type, *pp2a-b′γ* and *pp2a-b′γ P35S::PP2A-B′γ* samples.

Table S3. Proteins migrating below the 40-kDa gel band in wild-type, *pp2a-b′γ* and *pp2a-b′γ P35S::PP2A-B′γ* samples.

Table S4. Primers used for cloning of the bimolecular fluorescence complementation fusion protein expression constructs.

REFERENCES

Agerbirk, N., De Vos, M., Kim, J.H. and Jander, G. (2009) Indole glucosinolate breakdown and its biological effects. *Phytochem. Rev.* **8**, 101–120.

Alvarez, C., Angeles Bermudez, M., Romero, L.C., Gotor, C. and Garcia, I. (2012) Cysteine homeostasis plays an essential role in plant immunity. *New Phytol.* **193**, 165–177.

Amir, R. (2010) Current understanding of the factors regulating methionine content in vegetative tissues of higher plants. *Amino Acids*, **39**, 917–931.

Arasimowicz-Jelonek, M., Floryszak-Wieczorek, J., Gzyl, J. and Chmielowska-Bak, J. (2013) Homocysteine over-accumulation as the effect of potato leaves exposure to biotic stress. *Plant Physiol. Biochem.* **63**, 177–184.

Bednarek, P., Pislewska-Bednarek, M., Svatos, A. *et al.* (2009) A glucosinolate metabolism pathway in living plant cells mediates broad-spectrum antifungal defense. *Science*, **323**, 101–106.

Bednarek, P., Pislewska-Bednarek, M., van Themaat, E.V.L., Maddula, R.K., Svatos, A. and Schulze-Lefert, P. (2011) Conservation and clade-specific diversification of pathogen-inducible tryptophan and indole glucosinolate metabolism in *Arabidopsis thaliana* relatives. *New Phytol.* **192**, 713–726.

Bekaert, M., Edger, P.P., Hudson, C.M., Pires, J.C. and Conant, G.C. (2012) Metabolic and evolutionary costs of herbivory defense: systems biology of glucosinolate synthesis. *New Phytol.* **196**, 596–605.

Bender, J. and Fink, G.R. (1998) A Myb homologue, ATR1, activates tryptophan gene expression in Arabidopsis. *Proc. Natl Acad. Sci. USA* **95**, 5655–5660.

Brzezinski, K., Dauter, Z. and Jaskolski, M. (2012) High-resolution structures of complexes of plant S-adenosyl-L-homocysteine hydrolase (*Lupinus luteus*). *Acta Crystallogr. D. Struct. Biol.* **68**, 218–231.

Castro, R., Struys, E.A., Jansen, E.E.W., Blom, H.J., de Almeida, I.T. and Jakobs, C. (2002) Quantification of plasma S-adenosylmethionine and S-adenosylhomocysteine as their fluorescent 1, N-6-etheno derivatives: an adaptation of previously described methodology. *J. Pharm. Biomed. Anal.* **29**, 963–968.

Celenza, J.L., Quiel, J.A., Smolen, G.A., Merrikh, H., Silvestro, A.R., Normanly, J. and Bender, J. (2005) The Arabidopsis ATR1 Myb transcription factor controls indolic glucosinolate homeostasis. *Plant Physiol.* **137**, 253–262.

Clay, N.K., Adio, A.M., Denoux, C., Jander, G. and Ausubel, F.M. (2009) Glucosinolate metabolites required for an arabidopsis innate immune response. *Science*, **323**, 95–101.

Curien, G., Bastlen, O., Robert-Genthon, M., Cornish-Bowden, A., Cardenas, M.L. and Dumas, R. (2009) Understanding the regulation of aspartate metabolism using a model based on measured kinetic parameters. *Mol. Syst. Biol.* **5**, 271–285.

De Vos, M. and Jander, G. (2009) *Myzus persicae* (green peach aphid) salivary components induce defence responses in *Arabidopsis thaliana*. *Plant, Cell Environ.* **32**, 1548–1560.

Elmore, J.M., Liu, J., Smith, B., Phinney, B. and Coaker, G. (2012) Quantitative proteomics reveals dynamic changes in the plasma membrane during arabidopsis immune signaling. *Mol. Cell Proteomics* **11**. doi: 10.1074/mcp.M111.014555.

Fahey, R.C. and Newton, G.L. (1987) Determination of low-molecular-weight thiols using monobromobimane fluorescent labeling and high-performance liquid-chromatography. *Methods Enzymol.* **143**, 85–96.

Fahey, J.W., Zalcmann, A.T. and Talalay, P. (2001) The chemical diversity and distribution of glucosinolates and isothiocyanates among plants. *Phytochemistry*, **56**, 5–51.

Fan, J., Crooks, C., Creissen, G., Hill, L., Fairhurst, S., Doerner, P. and Lamb, C. (2011) Pseudomonas sax genes overcome aliphatic isothiocyanate-mediated non-host resistance in Arabidopsis. *Science*, **331**, 1185–1188.

Ferrer, J.L., Ravanel, S., Robert, M. and Dumas, R. (2004) Crystal structures of cobalamin-independent methionine synthase complexed with zinc, homocysteine, and methyltetrahydrofolate. *J. Biol. Chem.* **279**, 44235–44238.

Frerigmann, H., Boettcher, C., Baatout, D. and Gigolashvili, T. (2012) Glucosinolates are produced in trichomes of *Arabidopsis thaliana*. *Front. Plant Sci.* **3**, 242–255.

Frerigmann, H., Piślewska-Bednarek, M., Sánchez-Vallet, A., Molina, A., Glawischnig, E., Gigolashvili, T. and Bednarek, P. (2016) Regulation of pathogen triggered tryptophan metabolism in *Arabidopsis thaliana* by MYB transcription factors. *Mol. Plant*, **9**, 682–695.

Gigolashvili, T., Berger, B., Mock, H.-P., Mueller, C., Weisshaar, B. and Fluegge, U.-I. (2007) The transcription factor HIG1/MYB51 regulates indolic glucosinolate biosynthesis in *Arabidopsis thaliana*. *Plant J.* **50**, 886–901.

Giovanelli, J., Mudd, S.H. and Datko, A.H. (1985) Quantitative-analysis of pathways of methionine metabolism and their regulation in lemna. *Plant Physiol.* **78**, 555–560.

Halkier, B.A. and Gershenzon, J. (2006) Biology and biochemistry of glucosinolates. *Annu. Rev. Plant Biol.* **57**, 303–333.

Ishihara, M., Kusakabe, Y., Ohsumichi, T., Tanaka, N., Nakanishi, M., Kitade, Y. and Nakamura, K.T. (2010) Crystallization of mouse S-adenosyl-L-homocysteine hydrolase. *Acta. Crystallogr. Sect. F. Struct. Biol. Cryst. Commun.* **66**, 313–315.

Ivanov, K.I., Eskelin, K., Basic, M., De, S., Lohmus, A., Varjosalo, M. and Mäkinen, K. (2016) Molecular insights into the function of the viral RNA silencing suppressor HCPro. *Plant J.* **85**, 30–45.

Jaspers, P., Blomster, T., Brosche, M. *et al.* (2009) Unequally redundant RCD1 and SRO1 mediate stress and developmental responses and interact with transcription factors. *Plant J.* **60**, 268–279.

Kangasjärvi, S., Lepistö, A., Hannikainen, K., Piippo, M., Luomala, E.-M., Aro, E.-M. and Rintamäki, E. (2008) Diverse roles for chloroplast stromal and thylakoid-bound ascorbate peroxidases in plant stress responses. *Biochem. J.* **412**, 275–285.

Kim, J.H. and Jander, G. (2007) *Myzus persicae* (green peach aphid) feeding on Arabidopsis induces the formation of a deterrent indole glucosinolate. *Plant J.* **49**, 1008–1019.

Konert, G., Trotta, A., Kouvonen, P., Rahikainen, M., Durian, G., Blokhina, O., Fagerstedt, K., Muth, D., Corthals, G.L. and Kangasjärvi, S. (2015a) Protein phosphatase 2A (PP2A) regulatory subunit B 'gamma interacts with cytoplasmic ACONITASE 3 and modulates the abundance of AOX1A and AOX1D in Arabidopsis thaliana. *New Phytol.* **205**, 1250–1263.

Konert, G., Rahikainen, M., Trotta, A., Durian, G., Salojärvi, J., Khorobrykh, S., Tyystjärvi, E. and Kangasjärvi, S. (2015b) Subunits B′γ and B′ζ of protein phosphatase 2A regulate photo-oxidative stress responses and growth in *Arabidopsis thaliana*. *Plant, Cell Environ.* **38**, 2641–2651.

Koroleva, O.A. and Cramer, R. (2011) Single-cell proteomic analysis of glucosinolate-rich S-cells in *Arabidopsis thaliana*. *Methods*, **54**, 413–423.

Kreft, O., Hoefgen, R. and Hesse, H. (2003) Functional analysis of cystathionine gamma-synthase in genetically engineered potato plants. *Plant Physiol.* **131**, 1843–1854.

Kroymann, J. (2011) Natural diversity and adaptation in plant secondary metabolism. *Curr. Opin. Plant Biol.* **14**, 246–251.

Lee, S., Doxey, A.C., McConkey, B.J. and Moffatt, B.A. (2012) Nuclear targeting of methyl-recycling enzymes in *Arabidopsis thaliana* is mediated by specific protein interactions. *Mol. Plant* **5**, 231–248.

Levy, M., Wang, Q.M., Kaspi, R., Parrella, M.P. and Abel, S. (2005) Arabidopsis IQD1, a novel calmodulin-binding nuclear protein, stimulates glucosinolate accumulation and plant defense. *Plant J.* **43**, 79–96.

Li, S., Mhamdi, A., Trotta, A., Kangasjaervi, S. and Noctor, G. (2014) The protein phosphatase subunit PP2A-B 'gamma is required to suppress day length-dependent pathogenesis responses triggered by intracellular oxidative stress. *New Phytol.* **202**, 145–160.

Li, X., Huang, L., Hong, Y., Zhang, Y., Liu, S., Li, D., Zhang, H. and Song, F. (2015) Co-silencing of tomato S-adenosylhomocysteine hydrolase genes confers increased immunity against *Pseudomonas syringae* pv. *tomato* DC3000 and enhanced tolerance to drought stress. *Front. Plant Sci.* **6**, 717–730.

Loizeau, K., Gambonnet, B., Zhang, G.-F., Curien, G., Jabrin, S., Van der Straeten, D., Lambert, W.E., Rebeille, F. and Ravanel, S. (2007) Regulation of one-carbon metabolism in arabidopsis: the N-terminal regulatory domain of cystathionine gamma-synthase is cleaved in response to folate starvation. *Plant Physiol.* **145**, 491–503.

Loizeau, K., De Brouwer, V., Gambonnet, B., Yu, A., Renou, J.-P., Van Der Straeten, D., Lambert, W.E., Rebeille, F. and Ravanel, S. (2008) A genome-wide and metabolic analysis determined the adaptive response of Arabidopsis cells to folate depletion induced by methotrexate. *Plant Physiol.* **148**, 2083–2095.

Mikkelsen, M.D. and Halkier, B.A. (2003) Metabolic engineering of valine- and isoleucine-derived glucosinolates in Arabidopsis expressing CYP79D2 from cassava. *Plant Physiol.* **131**, 773–779.

Moffatt, B.A. and Weretilnyk, E.A. (2001) Sustaining S-adenosyl-L-methionine-dependent methyltransferase activity in plant cells. *Physiol. Plantarum* **113**, 435–442.

Moffatt, B.A., Stevens, Y.Y., Allen, M.S., Snider, J.D., Pereira, L.A., Todorova, M.I., Summers, P.S., Weretilnyk, E.A., Martin-McCaffrey, L. and Wagner, C. (2002) Adenosine kinase deficiency is associated with developmental abnormalities and reduced transmethylation. *Plant Physiol.* **128**, 812–821.

Nour-Eldin, H.H., Andersen, T.G., Burow, M., Madsen, S.R., Jorgensen, M.E., Olsen, C.E., Dreyer, I., Hedrich, R., Geiger, D. and Halkier, B.A. (2012) NRT/PTR transporters are essential for translocation of glucosinolate defence compounds to seeds. *Nature*, **488**, 531–534.

Ouyang, B., Fei, Z., Joung, J.-G. *et al.* (2012) Transcriptome profiling and methyl homeostasis of an Arabidopsis mutant deficient in S-adenosylhomocysteine hydrolase1 (SAHH1). *Plant Mol. Biol.* **79**, 315–331.

Pavet, V., Quintero, C., Cecchini, N.M., Rosa, A.L. and Alvarez, M.E. (2006) Arabidopsis displays centromeric DNA hypomethylation and cytological alterations of heterochromatin upon attack by *Pseudomonas syringae*. *Mol. Plant Microbe Intert.* **19**, 577–587.

Peters, K., Belt, K. and Braun, H.-P. (2013) 3D gel map of Arabidopsis complex I. *Front. Plant Sci.* **4**, 153–162.

Pfalz, M., Vogel, H. and Kroymann, J. (2009) The gene controlling the indole glucosinolate modifier1 quantitative trait locus alters indole glucosinolate structures and aphid resistance in Arabidopsis. *Plant Cell*, **21**, 985–999.

Pfalz, M., Mikkelsen, M.D., Bednarek, P., Olsen, C.E., Halkier, B.A. and Kroymann, J. (2011) Metabolic engineering in *Nicotiana benthamiana* reveals key enzyme functions in Arabidopsis indole glucosinolate modification. *Plant Cell*, **23**, 716–729.

Rasool, B., Karpinska, B., Konert, G., Durian, G., Denessiouk, K., Kangasjärvi, S. and Foyer, C.H. (2014) Effects of light and the regulatory B-subunit composition of protein phosphatase 2A on the susceptibility of *Arabidopsis thaliana* to aphid (*Myzus persicae*) infestation. *Front. Plant Sci.* **5**, 405.

Ravanel, S., Gakiere, B., Job, D. and Douce, R. (1998) The specific features of methionine biosynthesis and metabolism in plants. *Proc. Natl Acad. Sci. USA* **95**, 7805–7812.

Ravanel, S., Block, M.A., Rippert, P., Jabrin, S., Curien, G., Rebeille, F. and Douce, R. (2004) Methionine metabolism in plants - Chloroplasts are autonomous for de novo methionine synthesis and can import S-adenosylmethionine from the cytosol. *J. Biol. Chem.* **279**, 22548–22557.

Reddy, M.C.M., Kuppan, G., Shetty, N.D., Owen, J.L., Ioerger, T.R. and Sacchettini, J.C. (2008) Crystal structures of *Mycobacterium tuberculosis* S-adenosyl-L-homocysteine hydrolase in ternary complex with substrate and inhibitors. *Protein Sci.* **17**, 2134–2144.

Rocha, P., Sheikh, M., Melchiorre, R., Fagard, M., Boutet, S., Loach, R., Moffatt, B., Wagner, C., Vaucheret, H. and Furner, I. (2005) The Arabidopsis *HOMOLOGY-DEPENDENT GENE SILENCING1* gene codes for an S-adenosyl-L-homocysteine hydrolase required for DNA methylation-dependent gene silencing. *Plant Cell*, **17**, 404–417.

Roje, S., Wang, H., McNeil, S.D., Raymond, R.K., Appling, D.R., Shachar-Hill, Y., Bohnert, H.J. and Hanson, A.D. (1999) Isolation, characterization, and functional expression of cDNAs encoding NADH-dependent methylenetetrahydrofolate reductase from higher plants. *J. Biol. Chem.* **274**, 36089–36096.

Schlaeppi, K., Abou-Mansour, E., Buchala, A. and Mauch, F. (2010) Disease resistance of Arabidopsis to *Phytophthora brassicae* is established by the sequential action of indole glucosinolates and camalexin. *Plant J.* **62**, 840–851.

Slaymaker, D.H., Navarre, D.A., Clark, D., del Pozo, O., Martin, G.B. and Klessig, D.F. (2002) The tobacco salicylic acid-binding protein 3 (SABP3) is the.chloroplast carbonic anhydrase, which exhibits antioxidant activity and plays a role in the hypersensitive defense response. *Proc. Natl Acad. Sci. USA* **99**, 11640–11645.

Smith, C.M. and Clement, S.L. (2012) Molecular bases of plant resistance to arthropods. *Annu. Rev. Entomol.* **57**, 309–328.

Sønderby, I.E., Geu-Flores, F. and Halkier, B.A. (2010) Biosynthesis of glucosinolates - gene discovery and beyond. *Trends Plant Sci.* **15**, 283–290.

Stuttmann, J., Hubberten, H.-M., Rietz, S., Kaur, J., Muskett, P., Guerois, R., Bednarek, P., Hoefgen, R. and Parker, J.E. (2011) Perturbation of arabidopsis amino acid metabolism causes incompatibility with the adapted biotrophic pathogen *Hyaloperonospora arabidopsidis*. *Plant Cell*, **23**, 2788–2803.

Trotta, A., Wrzaczek, M., Scharte, J. *et al.* (2011) Regulatory subunit B′ gamma of protein phosphatase 2A prevents unnecessary defense reactions under low light in Arabidopsis. *Plant Physiol.* **156**, 1464–1480.

Trotta, A., Rahikainen, M., Konert, G., Finazzi, G. and Kangasjärvi, S. (2014) Signalling crosstalk in light stress and immune reactions in plants. *Philos. Trans. R. Soc. Lond. B Biol. Sci.* **369**. doi: 10.1098/rstb.2013.0235.

Trotta, A., Suorsa, M., Rantala, M., Lundin, B. and Aro, E.M. (2016) Serine and threonine residues of plant STN7 kinase are differentially phosphorylated upon changing light conditions and specifically influence the activity and stability of the kinase. *Plant J.* **87**, 484–494.

Van Wilder, V., De Brouwer, V., Loizeau, K. *et al.* (2009) C1 metabolism and chlorophyll synthesis: the Mg-protoporphyrin IX methyltransferase activity is dependent on the folate status. *New Phytol.* **182**, 137–145.

Waadt, R. and Kudla, J. (2008) In planta visualization of protein interactions using bimolecular fluorescence complementation (BiFC). *CSH Protoc.* pdb.prot4995-pdb.prot4995.

Walter, M., Chaban, C., Schutze, K. *et al.* (2004) Visualization of protein interactions in living plant cells using bimolecular fluorescence complementation. *Plant J.* **40**, 428–438.

Wienkoop, S., Zoeller, D., Ebert, B., Simon-Rosin, U., Fisahn, J., Glinski, M. and Weckwerth, W. (2004) Cell-specific protein profiling in *Arabidopsis thaliana* trichomes: identification of trichome-located proteins involved in sulfur metabolism and detoxification. *Phytochemistry*, **65**, 1641–1649.

Winterberg, B., Du Fall, L.A., Song, X., Pascovici, D., Care, N., Molloy, M., Ohms, S. and Solomon, P.S. (2014) The necrotrophic effector protein SnTox3 re-programs metabolism and elicits a strong defence response in susceptible wheat leaves. *BMC Plant Biol.* **14**, 215–230.

Xu, J., Meng, J., Meng, X., Zhao, Y., Liu, J., Sun, T., Liu, Y., Wang, Q. and Zhang, S. (2016) Pathogen-responsive MPK3 and MPK6 reprogram the biosynthesis of indole glucosinolates and their derivatives in arabidopsis immunity. *Plant Cell*, **28**, 1144–1162.

Zhang, H., Deng, X., Miki, D., Cutler, S., La, H., Hou, Y.-J., Oh, J. and Zhu, J.-K. (2012) Sulfamethazine suppresses epigenetic silencing in Arabidopsis by impairing folate synthesis. *Plant Cell*, **24**, 1230–1241.

Zhao, Y., Wang, J., Liu, Y. *et al.* (2015) Classic myrosinase-dependent degradation of indole glucosinolate attenuates fumonisin B1-induced programmed cell death in Arabidopsis. *Plant J.* **81**, 920–933.

Zhou, H.-R., Zhang, F.-F., Ma, Z.-Y., Huang, H.-W., Jiang, L., Cai, T., Zhu, J.-K., Zhang, C. and He, X.-J. (2013) Folate polyglutamylation is involved in chromatin silencing by maintaining global DNA methylation and histone H3K9 dimethylation in Arabidopsis. *Plant Cell*, **25**, 2545–2559.

Zubieta, C., He, X.Z., Dixon, R.A. and Noel, J.P. (2001) Structures of two natural product methyltransferases reveal the basis for substrate specificity in plant O-methyltransferases. *Nat. Struct. Biol.* **8**, 271–279.